All-optical switching in Cr- and Mn-doped L1$_0$ FePt thin films

Martin Stiehl◉,[1] Stephan Wust◉,[1,*] Nataliia Schmidt◉,[2] Tobias Dannegger◉,[3] Johannes Seyd◉,[2]
Marco Berritta,[4] Peter M. Oppeneer,[4] Manfred Albrecht◉,[2] Ulrich Nowak◉,[3] and
Martin Aeschlimann[1]

[1]*Department of Physics and Research Center OPTIMAS, RPTU Kaiserslautern-Landau,
Kaiserslautern 67663, Germany*
[2]*Institute of Physics, University of Augsburg, Augsburg 86135, Germany*
[3]*Fachbereich Physik, Universität Konstanz, Konstanz 78457, Germany*
[4]*Department of Physics and Astronomy, Uppsala University, P.O. Box 516, Uppsala S-75120, Sweden*

Optical manipulation of the magnetization of thin films opens up exciting possibilities for ever-faster magnetic storage applications. In this context, L1$_0$ chemically ordered FePt thin films are of particular interest due to their high perpendicular magnetic anisotropy and their use as a storage material for heat-assisted magnetic recording devices. However, these materials are difficult to manipulate with external fields due to their high coercivity field. Thus, we want to explore the possibility of tailoring the properties of these materials to enable switching using all-optical techniques. While stochastic all-optical switching between partially magnetized states has been reported for undoped FePt thin films, we have investigated to what extent doping with third elements can influence the switching behavior. Reducing the saturation magnetization may be one way to facilitate all-optical switching. While this is expected with the introduction of additional elements, we also want to highlight the role of the inverse Faraday effect and the magnetic circular dichroism in stochastic all-optical switching. In this study, Cr was found to be a promising dopant, which can almost double the relative magnetization change of the partially magnetized states compared to pure FePt.

I. INTRODUCTION

The manipulation of magnetization by external stimuli is a topic of great interest from a fundamental and application point of view, especially with respect to magnetic data-storage applications. In particular, L1$_0$ chemically ordered FePt thin films are of interest due to their large perpendicular magnetic anisotropy (PMA) and are currently used as a storage material for heat-assisted magnetic recording (HAMR) [1–3]. However, this approach has the disadvantage that the magnetic grains must be heated in order to switch the magnetic state using a moderate external magnetic field. Although the heating and cooling cycle takes less than 1 ns, it is still an order of magnitude longer than the magnetization dynamics induced by ultrashort optical pulses, which manipulate the magnetization on a subpicosecond timescale [4] and even induce magnetization reversal.

Helicity-dependent all-optical switching (HDAOS) was first discovered in ferrimagnetic Gd-Fe-Co thin films [5] but was soon found in a wide variety of magnetic materials, such as other rare earth-3d transition metal (RE-TM) alloys [6–10] and RE-TM bilayers [11,12], as well as antiferromagnetically coupled heterostructures [13,14]. Later on, HDAOS was even found in ferromagnetic materials, such as granular L1$_0$ FePt-Ag-C thin films, though only following a series of many laser pulses [15]. With the aim to uncover the origin of switching in FePt, further studies on granular L1$_0$ FePt thin films [16,17] revealed the stochastic nature of this switching process biased by a combination of the inverse Faraday effect (IFE) [8] and magnetic circular dichroism (MCD) giving rise to a thermal "reptationlike" effect [18].

In this work, we aim to influence the mechanism of HDAOS in hard magnetic L1$_0$ FePt thin films by systematically modifying the magnetic properties through the incorporation of third elements. In particular, a reduced saturation magnetization was considered useful for AOS [19], as demonstrated in exchange-coupled TbFe/TbFe bilayers [20]. It is expected that for FePt alloys the insertion of third elements such as Cr and Mn, which couple antiferromagnetically to Fe, can efficiently reduce the saturation magnetization [6,7]. Our systematic study shows that Cr, which substitutes Fe in the L1$_0$ FePt lattice at low

*Corresponding author: wust@rptu.de

concentration, is the most promising dopant to improve HDAOS compared to undoped FePt.

II. SAMPLE PREPARATION AND CHARACTERIZATION

Different sample series of $L1_0$-FePt thin films with Cr and Mn have been prepared on MgO(001) substrates at elevated temperatures by dc magnetron cosputtering from individual targets requiring different optimizations, as presented in Table I. To prevent the thin films from oxidation, all samples were capped with a 3-nm-thick Al layer after cooling down the sample at room temperature. The relevant structural and magnetic properties for both sample series are briefly discussed in the following.

The 3d-transition elements Cr and Mn exhibit both a stable $L1_0$ phase in the corresponding binary phase diagrams with Pt. For Cr substitution, the lattice parameter in the [001] growth direction increases steadily from $L1_0$-FePt to $L1_0$-CrPt, confirming that the Cr atoms in the lattice occupy Fe sites. The observed high degree of chemical order and (001) orientation is associated with strong PMA, which persists up to a Cr content of 20 at. %, as summarized in the Appendix. Of particular interest is the reconfiguration of the spin arrangement in FePt with increasing Cr addition. In the dilute alloy with low Cr content, isolated Cr magnetic moments couple antiferromagnetically to the ferromagnetic Fe matrix, forming a ferrimagnetic system. With increasing Cr concentration, antiferromagnetically exchange-coupled Cr-Cr pairs begin to appear, increasing magnetic frustration and disorder, which leads to canting of adjacent magnetic moments, as shown by first-principles calculations. At higher Cr concentrations a frustrated ferrimagnetic order is established until the antiferromagnetic $L1_0$-CrPt phase is formed. A detailed study

TABLE I. List of investigated thin-film samples. Chemical composition (uncertainty ± 2 at. %) and film thickness (uncertainty ± 5%) were determined by Rutherford backscattering spectrometry.

Composition	x (nominal)	Dopant content (at. %)	Thickness (nm)	Reference
$Fe_{52}Pt_{48}$			10	[21]
$(Fe_{100-x}Cr_x)Pt$	11, 15, 20	6, 8, 11	9, 9, 10	[21]
$(Fe_{100-x}Mn_x)Pt$	12, 20, 28	7, 11, 15	9, 9, 9	

of the structural and magnetic properties of the $L1_0$-FePt thin films with Cr can be found in Ref. [21].

A similar behavior was observed for Mn doping. Also in this case, Mn replaces Fe in the $L1_0$ lattice, showing a gradual decrease in PMA with increasing Mn content (see Appendix), in agreement with results reported in the literature [22,23].

III. EXPERIMENTAL RESULTS

Figure 1(a) shows the optical Faraday microscopy setup used in the experiments to image the quasistatic changes in the magnetization of the samples. A collimated, linearly polarized white light source was used for imaging and a pulsed Ti:sapphire multipass amplifier for excitation.

Since many parameters have been shown to influence whether a material exhibits AOS or not, a large parameter space would need to be explored. However, in the experimental study presented here, we have limited ourselves by fixing some of the excitation parameters. In detail, the laser repetition rate (6 kHz), pulse length (40 fs), exciting photon energy (1.55 eV), spot size (approximately 70 μm), and initial sample temperature (approximately 300 K) were
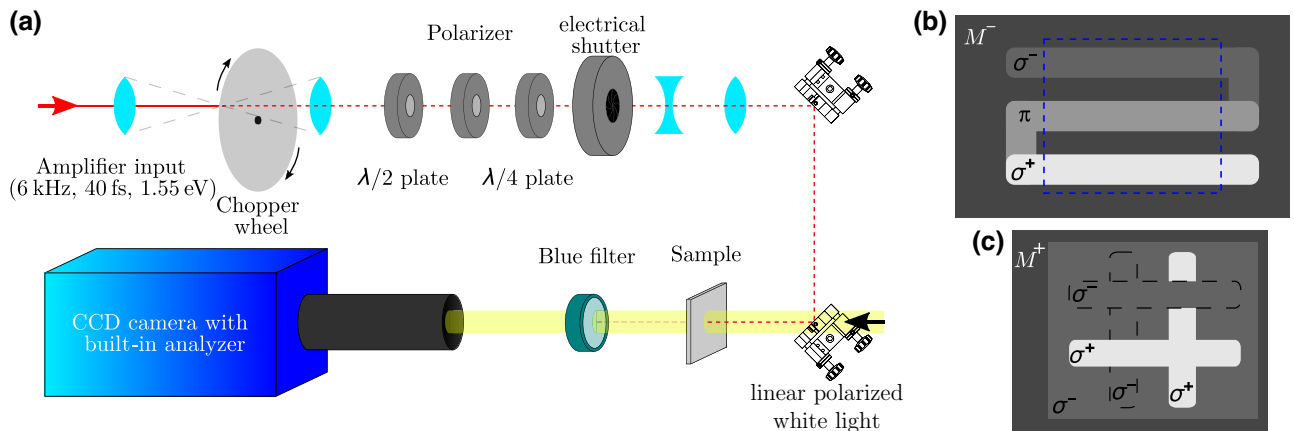

FIG. 1. (a) Schematic of the Faraday imaging setup used to measure light-induced quasistatic changes in magnetization. This setup consists of a broadband white-light source for imaging and a pulsed Ti:sapphire multipass amplifier for excitation of the system. For single-shot experiments the repetition rate of the excitation beam was reduced by a chopper wheel followed by an electrical shutter. (b) Schematic of the pattern used to evaluate the obtained contrast relative to the homogeneously magnetized initial state (M^-) when exposed to differently polarized light and its extended version (c) showing the different multiple illuminated regions.

kept constant, while the fluence of the exciting laser pulse was adjusted to a value that allowed a change in contrast for all three investigated light polarizations (circular polarization σ^+ and σ^-; linear polarization π).

To explore the influence of dopants on HDAOS, all samples were systematically investigated using the pattern shown in Fig. 1(b) to identify differences by sample illumination as a function of light polarization. For this purpose, the samples were first homogeneously magnetized in a strong external field to reach a defined initial state (M^-). Then the laser beam was written along three horizontal lines, changing the light polarization for each of them (σ^-, π, σ^+). Then, the difference images were calculated and the contrast profiles averaged along the vertical lines were extracted.

To study the helicity dependence in more detail, the test pattern was extended to the one shown in Fig. 1(c). To create this pattern, we started with a homogeneously magnetized background (M^+). On top of this background a rectangular area was prepared with σ^--polarized light to set a defined initial state (m^-). Then two horizontal lines were written, each line using a different circular polarization, σ^+ and σ^-, respectively. Afterwards, two vertical lines were written across the previously illuminated lines, again using the two circular polarizations. This allows us to extract contrast profiles at the intersections that indicate the influence of the initial states on the final state. To account for all possible combinations of initial state and illuminating light polarization, this pattern as well as the inverted version with the opposite background magnetization (M^-) and helicity (σ^+) for the illuminated area were prepared and analyzed.

A. Systematic switching study

First, we performed a systematic switching test using the pattern described in Fig. 1(b) for all samples with different dopant concentrations as listed in Table I.

The corresponding images and contrast profiles are shown in Fig. 2.

To quantify and compare these changes for the different dopants, we extract the contrast values c_{pol} corresponding to the different final states and calculate the difference Δc in image contrast relative to the initial state using

$$\Delta c = \frac{2|c_{\sigma^-} - c_{\sigma^+}|}{c_{\sigma^-} + c_{\sigma^+}}. \tag{1}$$

In Fig. 2(a) we can see that, for the undoped FePt sample, starting from a homogeneously saturated initial state M^- (contrast c set to zero), illumination with different light polarizations leads to different final states, showing a maximum switching of 11%. This indicates that, in the multishot experiment operating at 6 kHz, switching between two partially magnetized magnetic states occurs, as the contrast
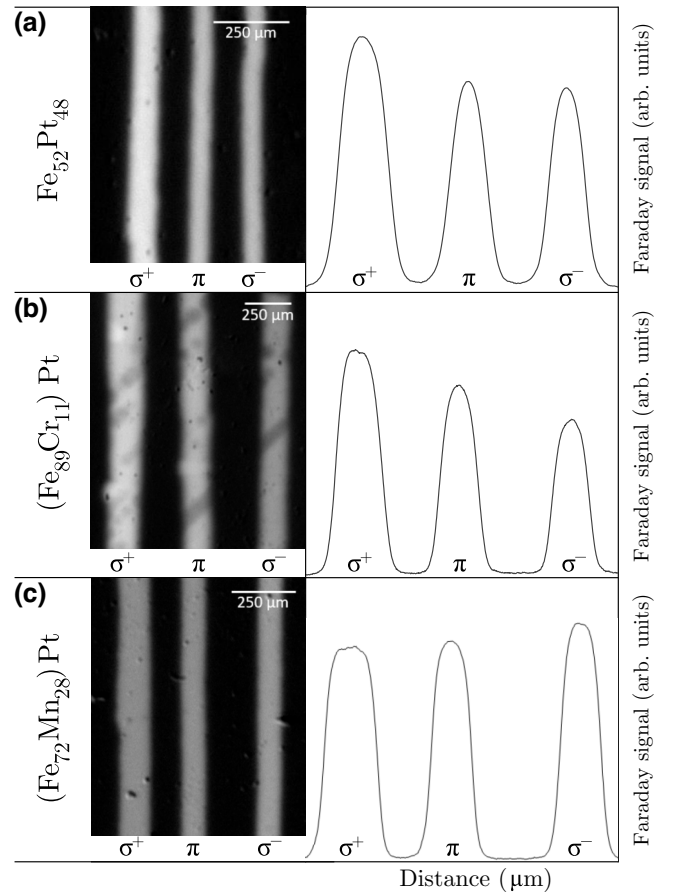

FIG. 2. Difference images using the pattern shown in Fig. 1(b) for a few selected samples of all the dopants used, with the concentrations that show the highest contrast. On the right are the extracted contrast profiles used to evaluate the achievable changes in magnetization upon illumination for the three written lines using different polarizations.

obtained by illumination with π-polarized light is nearly centered between those for circular polarization.

For the doped samples we find generally lower contrast values compared to pure FePt, as summarized in Fig. 3. Only for the Fe-Cr-Pt sample with 6 at. % Cr a nearly doubled relative contrast difference of about 19% can be found, which decreases to about 3% by increasing the Cr content to 8 at. %. For even higher contents, a slight increase can be found, similar to that for Mn doping, but the contrast values are still low and remain below the value for undoped FePt.

B. Fluence dependence

Since the $(Fe_{89}Cr_{11})Pt$ thin film revealed the largest helicity-dependent contrast, we investigated the origin of this contrast in more detail. To verify whether the switching results in a fixed final state or is fluence dependent, we plotted the obtained contrast against the applied fluence. The contrasts for all three polarizations are shown
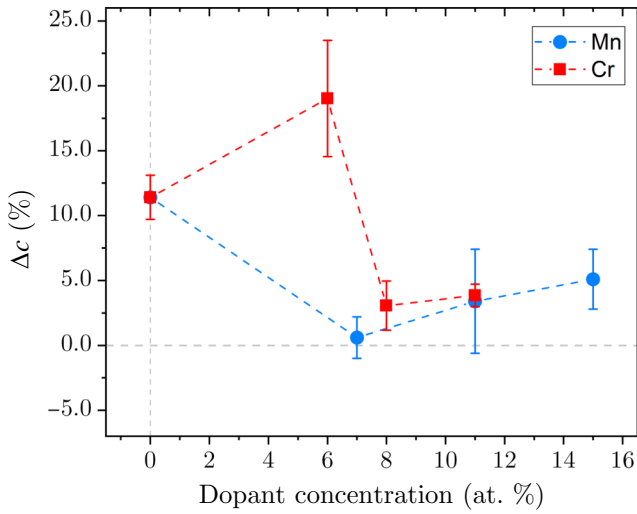
FIG. 3. The difference in contrast Δc between the areas illuminated with σ^+ and σ^- polarized light.

in Fig. 4(a). We see a clear effect of illumination only after a certain threshold fluence of about 1.3 mJ cm^{-2} is exceeded, independent of the light polarization. For intermediate fluences of 1.3 to 1.9 mJ cm^{-2}, the contrast builds up to an intermediate value. For fluences ≥1.9 mJ cm^{-2}, the contrast of the illuminated lines changes to a saturated level, which remains mostly constant for higher fluences. Only for significantly higher fluences (>5 mJ cm^{-2}), when the sample starts to get damaged, the contrast decreases again. This reduction can be explained by a higher optically induced sample temperature, which counteracts the switching process by favoring a random multidomain state [18]. Up to this fluence, one can see in the difference image shown in Fig. 4(b) that the width of the illuminated line increases with increasing applied fluence.

This implies that for applied fluences above the threshold of 1.3 mJ cm^{-2}, the final state depends only on the light polarization. Furthermore, for higher fluences above 1.9 mJ/cm^2, no change in contrast is observed until the destruction threshold is reached. This is in contrast to the findings of Takahashi *et al.* [16] for undoped FePt, who reported a continuously changing contrast with increasing laser fluence.

C. Influence of the initial state

In a next step, we tested the influence of the initial state on the final state using the extended pattern shown in Fig. 1(c) and its inverse version. The resulting difference images and extracted contrast profiles of the first written horizontal lines corresponding to a fixed initial state for the (Fe$_{89}$Cr$_{11}$)Pt sample are presented in Fig. 5. The value of zero in the left (right) contrast profiles corresponds to the initial magnetic state m^- (m^+) obtained by
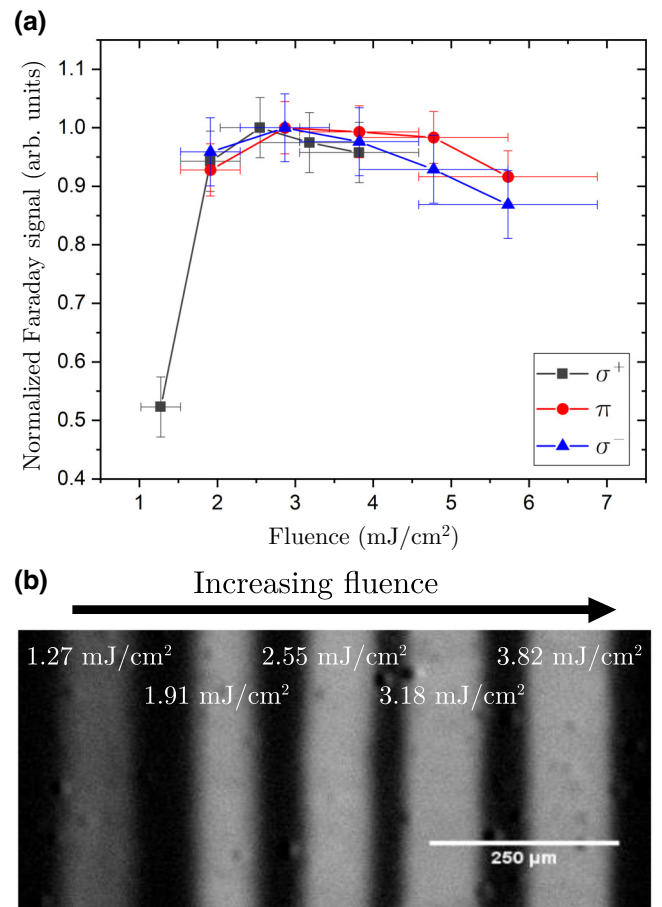
(a)

(b)

FIG. 4. (a) Contrast values for the three light polarizations (σ^+, π, and σ^-). The patterns for the different polarizations were generated at different sample locations, resulting in different illumination and thus different absolute Faraday signals. In order to better compare the different polarizations, the Faraday signal was normalized to 1. (b) Difference image of the (Fe$_{89}$Cr$_{11}$)Pt sample homogeneously magnetized to M^+ including lines written with σ^+-polarized light of increasing fluence from left to right.

illuminating the homogeneously magnetized sample with σ^- (σ^+) polarization.

Let us start with the difference images for both the pattern on the left and its inverse version on the right of Fig. 5. It can be seen that illuminating the initial state prepared with a certain light helicity with the corresponding opposite helicity ($\sigma^+\sigma^-$, $\sigma^-\sigma^+$) leads to a clearly visible change in contrast. However, illuminating with the same helicity ($\sigma^+\sigma^+$, $\sigma^-\sigma^-$) does not lead to any visible changes.

In order to quantify these observations, we analyze the extracted contrast profiles shown in Fig. 5. Within the noise level, the contrast values of the final states depend only on the polarization of the illuminating light. For example, if the contrast profiles of the marked horizontal lines are extracted from the left difference image and the cross sections with the vertical line written with σ^-
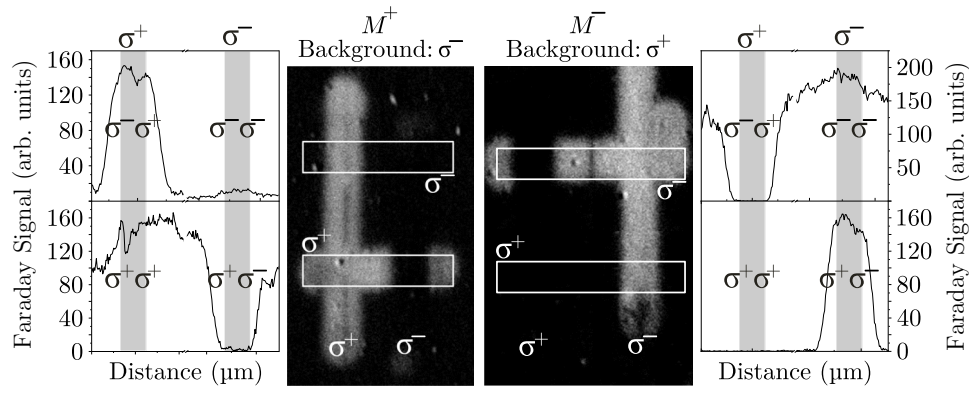
FIG. 5.   Shown are the results of applying the pattern sketched in Fig. 1(c) (left) and its inverse version (right) to the $(Fe_{89}Cr_{11})Pt$ sample. The contrast profiles adjacent to the images are extracted from the first written horizontal lines marked in the images.

polarization ($\sigma^-\sigma^-$, $\sigma^+\sigma^-$) are analyzed, we find a similar contrast value close to zero for both crossings. Evaluating the crossings with the other vertical line written with σ^+ polarization ($\sigma^-\sigma^+$, $\sigma^+\sigma^+$), yields a contrast value of about 160 [24]. Performing the analogous investigation for the inverse pattern on the right side, we obtain similar values of 0 and 160 for the cross sections with the vertical lines written with σ^+ and σ^- polarization, respectively [25].

The extracted contrast values thus confirm the qualitative observation that the final state is predominantly determined by the light polarization and not by the initial magnetic state.

Further considering that the homogeneously magnetized states M^+ and M^- are centered around the fully demagnetized state, corresponding to $M = 0$, we can assume that the partially magnetized states are also centered around the fully demagnetized state.

All these observations lead to the four-level scheme sketched in Fig. 6, which is supported by (i) the
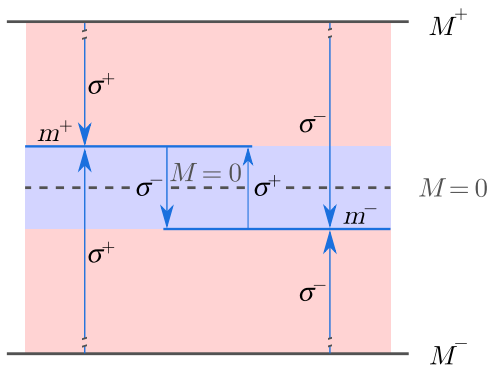
observation of a constant contrast difference between the regions illuminated by the two helicities, independent of the initial fully magnetized state, and (ii) the effectively reversed role of the two helicities for opposite homogeneously magnetized initial states (M^+ or M^-). Consequently, the previously extracted contrast difference Δc of the $(Fe_{89}Cr_{11})Pt$ sample can be used to determine the relative magnetization of the partially magnetized states as $m^\pm = (\Delta c/2)\, M^\pm = 0.18\, M^\pm$, which is nearly double the value found for undoped FePt ($m^\pm_{FePt} = 0.11\, M^\pm$).

This result is consistent with reports by Refs. [16,17], where the measured contrast is interpreted in terms of switching probabilities of more or less magnetically independent grains. While in the initial states (M^+ or M^-) these grains are mostly magnetized in one field direction, each laser pulse leads to thermal activation and thus to random switching of individual grains. This alone would lead—on average—to complete demagnetization. The IFE, however, favors one of the orientations in a helicity-dependent manner. After a large number of laser pulses, the accumulated switching probabilities of the individual grains, averaged over the laser-spot size, lead to the magnetized states $m^\pm$. These states do not depend on the initial condition, but they are also not completely magnetized, since each laser pulse with its heating effect can also lead to a switching in the wrong direction for some of the grains [17]. This is especially true for smaller grains. On the other hand, very large grains are difficult to switch and may not follow the IFE at all, since some degree of thermal activation may help to overcome the anisotropy energy barrier.

A direct comparison of the grain sizes of the different papers suggests that smaller grains result in more efficient switching.

To further improve this effect, the layer thickness could be optimized, as reported for example by Lambert et al. [15] on Co/Pt multilayers. Following this approach, by measuring the contrast in a wedged $(Fe_{89}Cr_{11})Pt$ sample

FIG. 6.   Sketch of the proposed model describing the observed switching between the partially magnetized states (m^+ and m^-), centered around the state with $M = 0$ (equal amount of up and down magnetized grains).

over a thickness range of 0 to 20 nm, an increase in contrast difference towards lower thicknesses was indeed observed (not shown). However, the absolute contrast values decreased sharply, so that no optimal film thickness could be determined due to the increasing noise. However, these measurements may explain the different levels of relative magnetization switching reported for undoped FePt [16,17], since the film thicknesses, as well as the grain sizes, are quite different. While John *et al.* do not report the grain size directly, they assume a grain volume of $(5 \text{ nm})^3$ in their calculations. Takahashi *et al.* report an average grain size of 11.99 nm and a film thickness of 10 nm. In contrast, our sample has a film thickness of 10 nm but a much larger grain size of about 150 nm [21], suggesting the possibility of further increasing contrast by optimizing these quantities.

D. Single-shot experiments

So far, all multishot experiments have been performed at a laser repetition rate of 6 kHz. However, the most desirable improvement of the material would be the transition from stochastic HDAOS, as observed in undoped FePt, to deterministic HDAOS. This would allow the magnetization of the irradiated region to be changed with a single pulse.

For this purpose, we performed single-shot experiments using a pulse length of 40 fs, a photon energy of 1.55 eV, a spot size of 120 μm, and a fluence of 5.7 mJ cm^{-2}. The experiment was carried out in a similar way to the one with the pattern in Fig. 1(b). The sample was homogeneously magnetized in the M^+ state and a large area was illuminated with σ^--polarized light (m^-) to highlight the contrast changes. The laser pulses were then applied to the sample, with an image taken after each pulse. We chose a series of pulses in which we first apply three individual σ^--polarized pulses to show that the initial state is a saturated state, followed by three single σ^+-polarized

pulses attempting to switch from m^- to m^+, and then three additional single σ^--polarized pulses attempting to switch from m^+ back to m^-.

The result of this procedure applied to the $(\text{Fe}_{89}\text{Cr}_{11})\text{Pt}$ sample is presented in Fig. 7. Here we can see that, when illuminating with σ^--polarized light pulses, no change in contrast can be observed, thus the region remains in the m^- state. Subsequently, applying pulses of the opposite helicity (σ^+), a strong change in contrast towards m^+ is observed. However, successive pulses further increase the contrast, indicating that the observed switching is an accumulative process. Irradiating the partially switched area with σ^--polarized light switches it back to the initial state m^-. But again, one pulse is not sufficient to fully return to the initial state. These observations confirm a stochastic HDAOS process as a reversal mechanism.

IV. OPTOMAGNETIC PROPERTIES

We have seen that HDAOS in FePt can be enhanced by doping with Cr but is diminished by doping with Mn. To shed some light on the reason for this difference, we can start by looking at *ab initio* calculated data on the magnetic circular dichroism (MCD) and the inverse Faraday effect (IFE) in the undoped materials FePt, CrPt, and MnPt. All three materials have the L1$_0$ structure. While FePt is an easy-axis ferromagnet, CrPt and MnPt are both easy-plane antiferromagnets.

For the purely antiferromagnetic systems CrPt and MnPt, the MCD has to vanish because they have no finite net magnetization. The IFE however does not vanish in antiferromagnets despite the symmetry of the sublattices. This was shown previously by *ab initio* calculations on CrPt [26] [data shown in Fig. 9(c)] and here, we present the same calculations for MnPt [see Fig. 9(d)] based on the same *ab initio* framework [27].
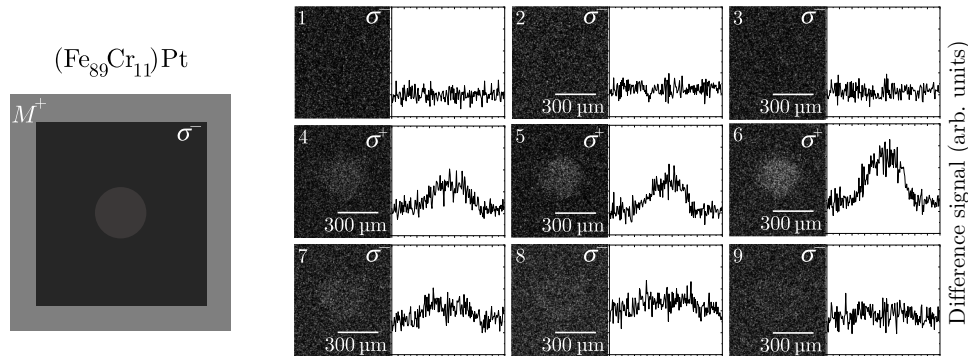

FIG. 7. Sketch of the pattern used in the single-shot experiment in conjunction with the different images and extracted contrast profiles highlighting the changes caused by the application of single-laser pulses. The following single-pulse sequence was chosen: $\sigma^-, \sigma^-, \sigma^-/\sigma^+, \sigma^+, \sigma^+/\sigma^-, \sigma^-, \sigma^-$ (1-9). Each image shows the polarization of the applied single pulse and the sequence number at the top.

This framework has also been used to calculate *ab initio* MCD and IFE data for FePt [17], which is reproduced in Figs. 9(a) and 9(b).

A. Magnetic circular dichroism

Since FePt is a ferromagnet, the MCD is not generally zero, but the *ab initio* data show that the photon energy used in the experiment happens to coincide with a sign change in the MCD, and thus it is rather small here as well. A possible explanation for the improved switching probability in Cr-doped FePt could therefore be caused by an increase in the MCD introduced by the doping.

In order to investigate this, we measured the normalized MCD-contrast of the alloys directly using optical methods. This was done by measuring the absorbed power a for both helicities (σ^+, σ^-) and subtracting the reflected and transmitted power from the total applied power. All measurements were performed under normal incidence. The normalized MCD-contrast c_{MCD} is then calculated by

$$c_{MCD} = \frac{a_{\sigma^-} - a_{\sigma^+}}{a_{\sigma^-} + a_{\sigma^+}}. \qquad (2)$$

The results shown in Fig. 8 are indeed revealing an increase of c_{MCD} for Cr- and the Mn-doped FePt alloys with a maximum at the lowest dopant concentration. Particularly in the case of Cr, we find a doubling of c_{MCD} when we move from pure FePt to 6 at. % doping, which underpins our assumption that this could be a reason for the enhanced switching probability in Cr-doped FePt. However, in Fig. 8 we can see the same trend for the Mn-doped FePt alloys, but no enhanced switching probability in the previously shown experiments (Fig. 3).
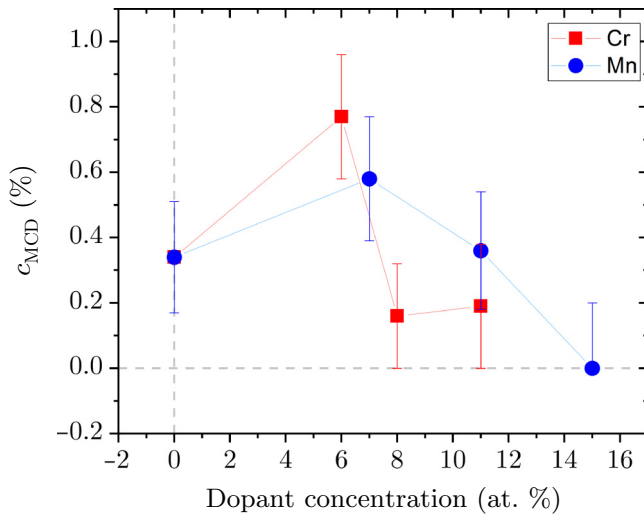

FIG. 8. Normalized MCD-contrast c_{MCD} in dependence of the dopant concentration for Cr- and Mn-doped FePt alloys.

B. Inverse Faraday effect

In our *ab initio* framework, the magnetic moments induced by the IFE are defined as

$$\mu_{ind} = \frac{K_{IFE}(\omega)I}{c_v}, \qquad (3)$$

where I is the laser intensity, K_{IFE} the IFE constant, and c_v the speed of light.

To get a first idea about the influence of doping on the IFE, we start with the simplified assumption that the induced magnetic moments on each atom in the doped materials would be the same as they would be in the corresponding pure material. The magnitude and sign of the induced magnetic moments depend on the photon energy, helicity, and local magnetization. For the photon energy of 1.55 eV used in the experiment, the specific computed values are given in Table II.

The induced magnetic moments can also be separated into spin and orbital contributions for each atom type. For our purposes here, we consider only the sum of spin and orbital moments. The values given in Fig. 9 refer to the sum of induced moments for Pt and Fe/Cr/Mn.

For relatively low dopant concentrations, the third element's atomic magnetic moments are aligned antiparallel to those of Fe, as they couple antiferromagnetically. Hence

TABLE II. Symmetrized *ab initio* computed IFE values K_{IFE} in hT^{-1} for FePt, CrPt, and MnPt, separated by atom type, helicity, and orientation of the local magnetic moment for a photon energy of 1.55 eV. The sum of both Fe/Cr/Mn and Pt-induced moments are also shown, as well as the difference between the magnetic moments induced for both directions.

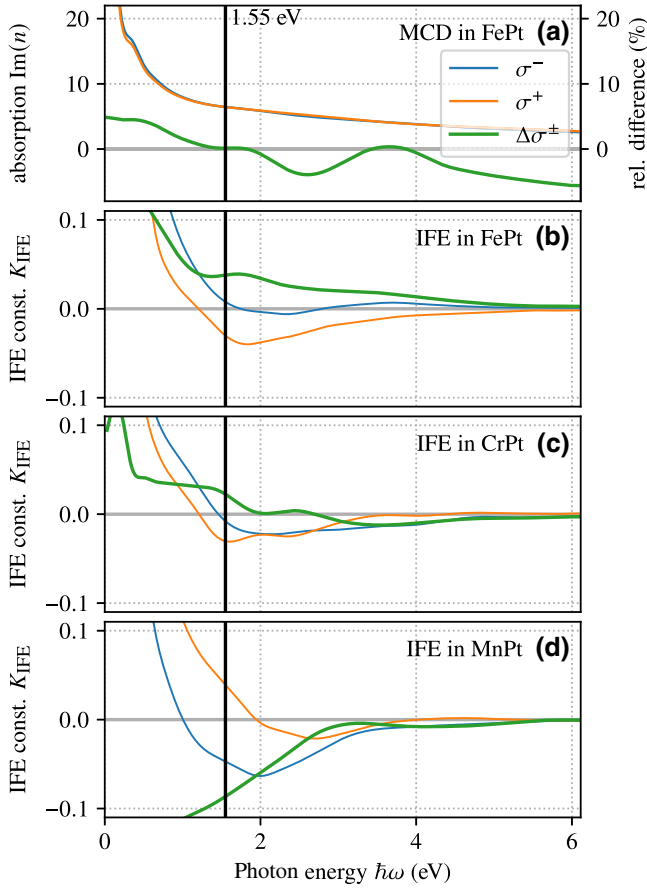|	FePt					
	Fe		Pt		Fe + Pt	
	σ^+	σ^-	σ^+	σ^-	σ^+	σ^-
↑	−2.5	0.3	3.2	−3.2	0.7	−2.9
↓	−0.3	2.5	3.2	−3.2	2.9	−0.7
$\Delta_{\uparrow\downarrow}$	−2.2	−2.2	0.0	0.0	−2.2	−2.2
	CrPt					
	Cr		Pt		Cr + Pt	
	σ^+	σ^-	σ^+	σ^-	σ^+	σ^-
↑	−4.6	0.6	1.6	−1.6	−3.0	−1.0
↓	−0.6	4.6	1.6	−1.6	1.0	3.0
$\Delta_{\uparrow\downarrow}$	−4.0	−4.0	0.0	0.0	−4.0	−4.0
	MnPt					
	Mn		Pt		Mn + Pt	
	σ^+	σ^-	σ^+	σ^-	σ^+	σ^-
↑	−1.6	0.8	5.4	−5.4	3.8	−4.6
↓	−0.8	1.6	5.4	−5.4	4.6	−3.8
$\Delta_{\uparrow\downarrow}$	−0.8	−0.8	0.0	0.0	−0.8	−0.8

FIG. 9. *Ab initio* calculations of the MCD and IFE values as a function of photon energy. Shown is (a) the helicity-dependent absorption of FePt, as well as (b)–(d) the IFE constants of FePt, CrPt, and MnPt. The green lines show (a) the relative difference between the two absorption coefficients in % and (b)–(d) the absolute difference between the IFE constants. The sign of the IFE constant corresponds to the sign of the induced moment relative to the atomic magnetic moment. The latter is oriented opposite to the incident light's $\vec{k}$ vector in (b) and parallel to it in (c) and (d). The black line indicates the photon energy used in the experiments.

in Fig. 9, we consider the IFE constants for antiparallel alignment with respect to the $\vec{k}$ vector of the laser light for FePt but parallel for CrPt and MnPt.

The given sign of the IFE constant is also relative to the atomic magnetic moment such that a positive sign indicates parallel alignment, which would reduce the switching probability, and a negative sign indicates opposite alignment, which would support the switching process. For a cumulative switching experiment with many laser pulses in succession, the equilibrium magnetization depends on the difference between both helicities, indicated by the green lines in Fig. 9. At the relevant photon energy of 1.55 eV, we see that this difference is almost the same in FePt and CrPt. For both materials, the IFE supports the switching
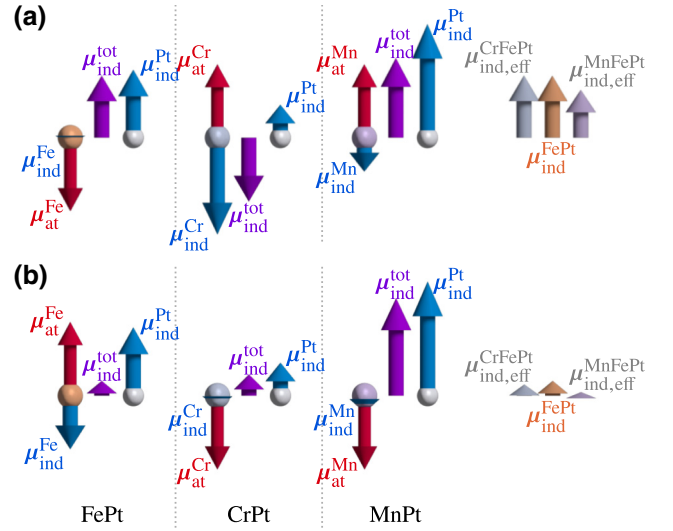

FIG. 10. Orientation and relative magnitude of the induced optomagnetic moments for the opposite initial magnetization at a photon energy of 1.55 eV. Shown are the values for (pure) FePt, CrPt, and MnPt with atomic magnetic moments (red) aligned in opposite directions for CrPt and MnPt compared to FePt. The induced magnetic moments are shown separately for each atom in blue while the resulting total induced moments ($\vec{\mu}_{ind}^{tot}$) are shown in purple. On the right, effective induced magnetic moments for the doped materials are compared to the induced moment in pure FePt. The induced magnetic moments are magnified by a factor of 20 relative to the atomic moments.

process. In MnPt, however, the difference is much larger and the sign is opposite compared to FePt.

This could explain why the cumulative switching probability is diminished in Mn-doped FePt. By combining the total induced magnetic moments $\vec{\mu}_{ind}^{FePt}$ and $\vec{\mu}_{ind}^{CrPt}$ or $\vec{\mu}_{ind}^{MnPt}$ from the undoped materials according to the atomic concentration c, we can naively compute an effective induced moment for the doped material as

$$\vec{\mu}_{ind,eff}^{CrFePt} = (1 - c) \cdot \vec{\mu}_{ind}^{FePt} - c \cdot \vec{\mu}_{ind}^{CrPt}, \qquad (4)$$

and analogously for Mn-doped FePt. This is also visualized in Fig. 10 for a concentration of 10%. Following this simple calculation, it appears that the addition of Mn atoms would decrease the effective induced moments compared to undoped FePt for both orientations and helicities. This behavior could also explain why we do not have an increased switching probability, although the MCD increases at low Mn concentrations.

The above argument hinges on the assumption that the *ab initio* results for the individual sublattices of the pure materials can be applied to the corresponding atoms in the doped materials. We cannot know *a priori* if this is true. Ab initio calculations on the doped materials could resolve this but would be much more computationally expensive and are unfortunately beyond the scope of this work.

C. Other effects

Overall, the increase of the MCD seems to be a key factor enhancing the switching efficiency, but the sign of the IFE constants might have a diminishing effect on the switching efficiency with Mn doping while supporting it with Cr. On top of that, there are other effects that might conceivably influence the switching process as well, which we briefly discuss in the following.

The atomic magnetic moment is nearly twice as large for Mn than for Cr. Since a larger magnetic moment is associated with slower spin dynamics, this might also lead to a reduced switching effectiveness with Mn compared to Cr, as the switching process occurs on ultrafast timescales. On the other hand, the larger moment of Mn leads to a larger decrease in the saturation magnetization, which may enhance the switching process.

While FePt, CrPt, and MnPt all have the same $L1_0$ structure, the lattice constants differ slightly. Compared to FePt, the tetragonal structure is elongated along the c axis for CrPt, resulting in a lower density, while slightly compressed for MnPt. Doping with these two materials could therefore alter the magnetocrystalline anisotropy of FePt in different ways, leading to a different switching efficiency.

Since ultrafast heating is involved in the switching process, another aspect to consider is how doping with different third elements influences the electronic and phononic heat capacity and the coupling between the heat baths.

V. SUMMARY

In this study, we systematically investigated the influence of doping $L1_0$ FePt thin films with third elements (Cr, Mn) on the optically induced switching behavior. We demonstrated that by adding 6 at. % of Cr, which substitutes Fe in the $L1_0$ FePt lattice, the maximum relative magnetization between areas illuminated with light of opposite circular polarization nearly doubles from 11 to 19% compared to pure FePt. The switching process is however still stochastic (and not deterministic), as evidenced by single-shot experiments. While many factors play a role in the modulation of the switching probability, *ab initio* data on the undoped materials suggests that the sign of the induced magnetic moments in MnPt compared to CrPt decides whether the IFE favors the switching probability or not. Along with the increasing MCD in both alloys, this could explain why switching in low-concentration-doped Cr-doped FePt is enhanced, while it is diminished with Mn doping.

All data needed to reach the conclusions shown in the paper will be available from the authors upon reasonable request.

ACKNOWLEDGMENTS

APPENDIX: MAGNETIC CHARACTERIZATION AND PROPERTIES

Figures 11 and 12 summarize the magnetic properties for the Fe-Pt-Mn and Fe-Pt-Cr series that are discussed in
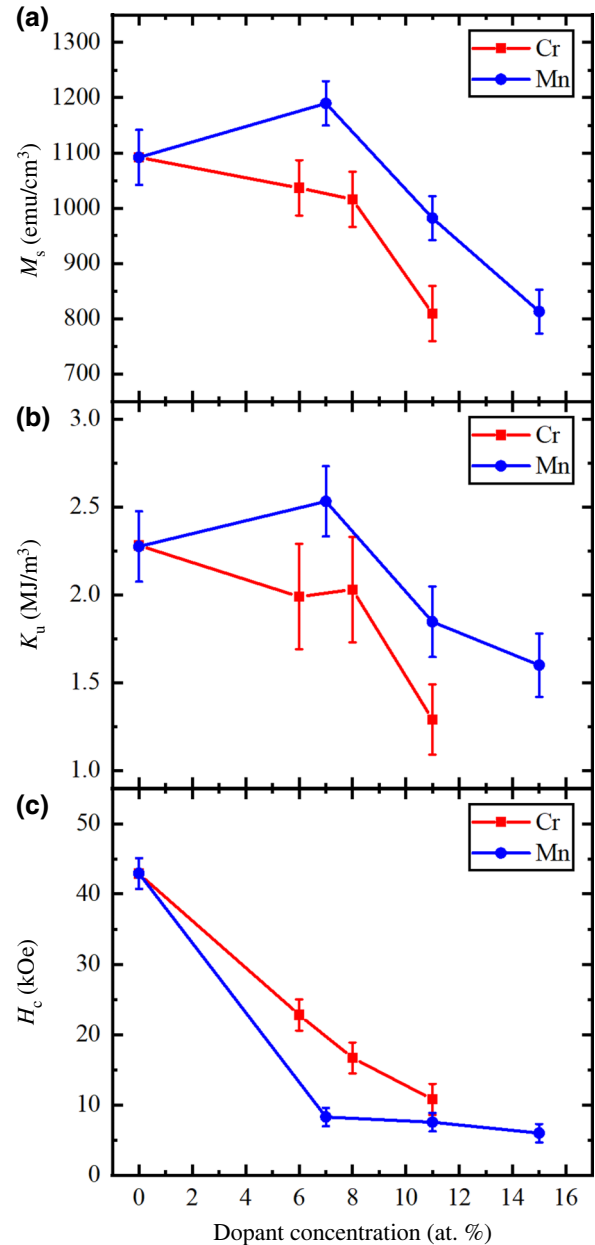

FIG. 11. (a) Saturation magnetization, (b) uniaxial anisotropy, and (c) coercive field as a function of dopant concentration for the Fe-Pt-Mn and the Fe-Pt-Cr series.
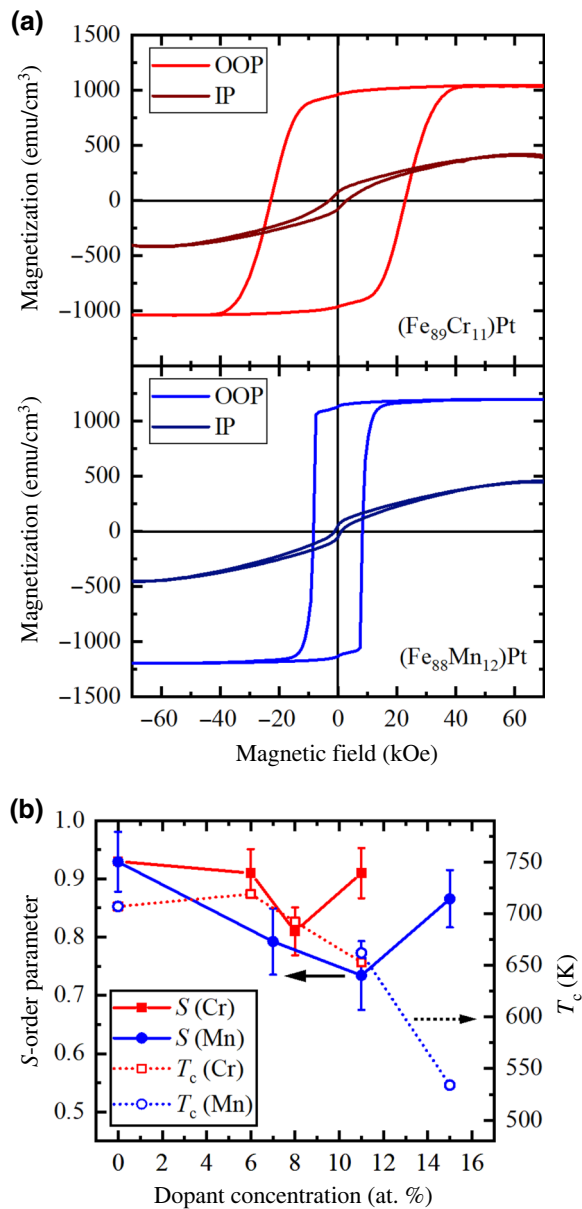
FIG. 12.   (a) *M-H* hysteresis loops measured in out-of-plane and in-plane geometry at 300 K for the Fe-Pt-Cr and Fe-Pt-Mn samples with the lowest Cr and Mn concentrations, respectively. (b) Curie temperature T_C and order parameter S as a function of Mn and Cr concentration.

the main paper. A detailed description on the characterization method as well as on the sample growth can be found in Ref. [21].

[1] D. Weller, G. Parker, O. Mosendz, A. Lyberatos, D. Mitin, N. Y. Safonova, and M. Albrecht, FePt heat assisted magnetic recording media, J. Vac. Sci. Technol. B **34**, 060801 (2016).

[2] M. Kief and R. Victora, Materials for heat-assisted magnetic recording, MRS Bull. **43**, 87 (2018).

[3] K. Hono, Y. Takahashi, G. Ju, J.-U. Thiele, A. Ajan, X. Yang, R. Ruiz, and L. Wan, Heat-assisted magnetic recording media materials, MRS Bull. **43**, 93 (2018).

[4] E. Beaurepaire, J.-C. Merle, A. Daunois, and J.-Y. Bigot, Ultrafast spin dynamics in ferromagnetic nickel, Phys. Rev. Lett **76**, 4250 (1996).

[5] C. D. Stanciu, F. Hansteen, A. V. Kimel, A. Kirilyuk, A. Tsukamoto, A. Itoh, and T. Rasing, All-optical magnetic recording with circularly polarized light, Phys. Rev. Lett **99**, 047601 (2007).

[6] A. Hassdenteufel, B. Hebler, C. Schubert, A. Liebig, M. Teich, M. Helm, M. Aeschlimann, M. Albrecht, and R. Bratschitsch, Thermally assisted all-optical helicity dependent magnetic switching in amorphous $Fe_{100-x}Tb_x$ alloy films, Adv. Mater. **25**, 3122 (2013).

[7] B. Hebler, A. Hassdenteufel, P. Reinhardt, H. Karl, and M. Albrecht, Ferrimagnetic Tb–Fe alloy thin films: Composition and thickness dependence of magnetic properties and all-optical switching, Front. Mater. **3**, 8 (2016).

[8] S. Alebrand, M. Gottwald, M. Hehn, D. Steil, M. Cinchetti, D. Lacour, E. E. Fullerton, M. Aeschlimann, and S. Mangin, Light-induced magnetization reversal of high-anisotropy TbCo alloy films, Appl. Phys. Lett. **101**, 162408 (2012).

[9] M. Finazzi, M. Savoini, A. Khorsand, A. Tsukamoto, A. Itoh, L. Duo, A. Kirilyuk, T. Rasing, and M. Ezawa, Laser-induced magnetic nanostructures with tunable topological properties, Phys. Rev. Lett. **110**, 177205 (2013).

[10] M. S. El Hadri, P. Pirro, C.-H. Lambert, S. Petit-Watelot, Y. Quessab, M. Hehn, F. Montaigne, G. Malinowski, and S. Mangin, Two types of all-optical magnetization switching mechanisms using femtosecond laser pulses, Phys. Rev. B **94**, 064412 (2016).

[11] A. Cao, Y. L. Van Hees, R. Lavrijsen, W. Zhao, and B. Koopmans, Dynamics of all-optically switched magnetic domains in Co/Gd heterostructures with Dzyaloshinskii-Moriya interaction, Phys. Rev. B **102**, 104412 (2020).

[12] M. Beens, M. L. Lalieu, A. J. Deenen, R. A. Duine, and B. Koopmans, Comparing all-optical switching in synthetic-ferrimagnetic multilayers and alloys, Phys. Rev. B **100**, 220409 (2019).

[13] S. Mangin, M. Gottwald, C. Lambert, D. Steil, V. Uhlíř, L. Pang, M. Hehn, S. Alebrand, M. Cinchetti, G. Malinowski, *et al.*, Engineered materials for all-optical helicity-dependent magnetic switching, Nat. Mater. **13**, 286 (2014).

[14] R. F. Evans, T. A. Ostler, R. W. Chantrell, I. Radu, and T. Rasing, Ultrafast thermally induced magnetic switching in synthetic ferrimagnets, Appl. Phys. Lett. **104**, 082410 (2014).

[15] C.-H. Lambert, S. Mangin, B. C. S. Varaprasad, Y. Takahashi, M. Hehn, M. Cinchetti, G. Malinowski, K. Hono, Y. Fainman, M. Aeschlimann, *et al.*, All-optical control of ferromagnetic thin films and nanostructures, Science **345**, 1337 (2014).

[16] Y. Takahashi, R. Medapalli, S. Kasai, J. Wang, K. Ishioka, S. Wee, O. Hellwig, K. Hono, and E. Fullerton, Accumulative magnetic switching of ultrahigh-density recording media by circularly polarized light, Appl. Phys. Lett. **6**, 054004 (2016).

[17] R. John, M. Berritta, D. Hinzke, C. Müller, T. Santos, H. Ulrichs, P. Nieves, J. Walowski, R. Mondal,

O. Chubykalo-Fesenko, *et al.*, Magnetisation switching of FePt nanoparticle recording medium by femtosecond laser pulses, Sci. Rep. **7,** 4114 (2017).

[18] M. O. Ellis, E. E. Fullerton, and R. W. Chantrell, All-optical switching in granular ferromagnets caused by magnetic circular dichroism, Sci. Rep. **6,** 30522 (2016).

[19] A. Hassdenteufel, J. Schmidt, C. Schubert, B. Hebler, M. Helm, M. Albrecht, and R. Bratschitsch, Low-remanence criterion for helicity-dependent all-optical magnetic switching in ferrimagnets, Phys. Rev. B **91,** 104431 (2015).

[20] C. Schubert, A. Hassdenteufel, P. Matthes, J. Schmidt, M. Helm, R. Bratschitsch, and M. Albrecht, All-optical helicity dependent magnetic switching in an artificial zero moment magnet, Appl. Phys. Lett. **104,** 082406 (2014).

[21] N. Y. Schmidt, R. Mondal, A. Donges, J. Hintermayr, C. Luo, H. Ryll, F. Radu, L. Szunyogh, U. Nowak, and M. Albrecht, $L1_0$-ordered $(Fe_{100-x}Cr_x)Pt$ thin films: Phase formation, morphology, and spin structure, Phys. Rev. B **102,** 214436 (2020).

[22] G. Meyer and J.-U. Thiele, Effective electron-density dependence of the magnetocrystalline anisotropy in highly chemically ordered pseudobinary $(Fe_{1-x}Mn_x)_{50}Pt_{50}L1_0$ alloys, Phys. Rev. B **73,** 214438 (2006).

[23] J.-C. A. Huang, Y. Chang, C. Yu, Y.-D. Yao, Y. Hu, and C. Fu, Mn doping effect on structure and magnetism of epitaxial $(FePt)_{1-x}Mn_x$ films, J. Appl. Phys. **93,** 8173 (2003).

[24] Mean values of $(148; 156 \,|\, 12; 3)$ for the intersections of the horizontal lines with the vertical lines ($\sigma^-\sigma^+$; $\sigma^+\sigma^+ | \sigma^-\sigma^-$; $\sigma^+\sigma^-$).

[25] Mean values of $(0; 0 \,|\, 186; 159)$.

[26] T. Dannegger, M. Berritta, K. Carva, S. Selzer, U. Ritzmann, P. M. Oppeneer, and U. Nowak, Ultrafast coherent all-optical switching of an antiferromagnet with the inverse Faraday effect, Phys. Rev. B **104,** L060413 (2021).

[27] M. Berritta, R. Mondal, K. Carva, and P. M. Oppeneer, Ab initio theory of coherent laser-induced magnetization in metals, Phys. Rev. Lett. **117,** 137203 (2016).